JOURNAL OF PROPULSION AND POWER
Vol. 23, No. 5, September–October 2007

Experiments and Simulations of the Freezing of Jet Fuel in Forced Flow

Rajee Assudani,* Jamie S. Ervin,† and Lee Riehl*
University of Dayton, Dayton, Ohio 45469-0210

DOI: 10.2514/1.23411

Under low-temperature environmental conditions, the cooling of aircraft fuel results in reduced fluidity with the potential for freezing. To study the freezing behavior of jet fuel under forced flow conditions, a quartz duct was fabricated. The duct walls were cooled below the solidification temperatures of JP-8 and JPTS fuel samples by means of an environmental chamber. Freezing was also simulated using computational fluid dynamics, and the validity of the calculations was established by comparing them with experimental measurements. As they were unavailable, the low-temperature properties of a sample of JPTS were measured experimentally and were used in the simulations. The calculated temperature and solidified area of the fuel inside the duct agree well with those values measured in the experiments. This work demonstrates that computational fluid dynamics techniques can potentially be used to predict the fuel holdup in aircraft fuel tanks. The effect of flow rate on solidification was also simulated, and it was found that lower flow rates result in relatively more solidification of the fuel than do higher flow rates. The simulations of the freezing behaviors of JP-8 and JPTS samples were found to have essentially the same value of morphology constant. However, the crystal structures of these two fuels were studied in experiments and were found to be very different. This shows the inability of the model to capture small-scale details like the crystal microstructure. However, this limitation is not fatal because the focus here is on the overall flow and freezing behavior of jet fuels.

Nomenclature

C	=	morphology constant, m^{-2}
C_0	=	Kozeny pore geometry constant, dimensionless
C^*	=	product $C\mu$, $kg/m^3 \cdot s$
C_p	=	specific heat, $J/kg \cdot K$
f_l	=	liquid mass fraction, dimensionless
f_s	=	solid mass fraction, dimensionless
H	=	liquid and solid enthalpy, J/kg
h	=	liquid enthalpy, J/kg
K	=	permeability, m^2
P	=	pressure, Pa
T	=	temperature, K
T_h	=	temperature when solidification starts, K
T_l	=	temperature when solidification is complete, K
$\boldsymbol{u}$	=	superficial velocity vector, m/s
$\boldsymbol{u}_f$	=	actual fluid velocity vector, m/s
ΔH	=	heat of fusion, J/kg
ΔH_e	=	effective heat of fusion, J/kg
λ	=	porosity, dimensionless
μ	=	absolute viscosity, $kg/m \cdot s$
Σ	=	interstitial surface area of the pores per unit volume of porous material, m^{-1}

I. Introduction

WITH extended flight duration and the prevalence of cold air masses along polar routes or at high altitudes, the potential exists for fuel freezing. As the fuel temperature decreases, fine wax crystals appear and increase in size and concentration on further cooling. With sufficient crystallization, there is the potential for catastrophic fuel system failure due to blocked filters, valves, and other flow passages. Hence, it is desirable to simulate jet fuel freezing by computational fluid dynamics (CFD) to study fuel system design and performance at low temperatures.

The simulation of jet fuel freezing by CFD is complicated because jet fuel is a mixture of thousands of different hydrocarbon species. Jet fuel primarily consists of normal alkanes, branched alkanes, cycloparaffins, olefins, and aromatics. In addition, the composition of individual jet fuel samples varies with the fuel source. Because each hydrocarbon has its own solidification temperature, jet fuel freezes over a range of temperatures, and solidified jet fuel mainly consists of larger normal alkanes [1]. In past work, researchers simulated the solidification of mixtures involving two or three compounds with known phase composition relationships [2]. Although those mixtures are much simpler in composition than jet fuel, there were several challenges in the simulations, like calculating heat transfer during molecular rearrangement due to solidification [2]. The problem of simulating jet fuel flow is more difficult for several reasons, such as the lack of published thermophysical properties at low temperatures [3]. Another complexity in the simulation of jet fuel flow behavior at low temperatures is that phase composition relationships for jet fuel are unavailable. Moreover, jet fuel forms a liquid-solid matrix during solidification, which is challenging to simulate. Thermodynamic models for solid-liquid phase equilibria for jet fuel are being developed [1]. Although these thermodynamic models have been employed to study the solid-liquid phase behavior of jet fuels, they have not been convenient for the prediction of the flow and heat transfer conditions involving jet fuel solidification.

There have been limited attempts using numerical methods to simulate the freezing of jet fuel. A previous one-dimensional heat transfer analysis of an external wing tank did not predict the heat transfer satisfactorily because the tank height was neglected [4]. Results from that study showed that tank height was important in the heat transfer and flow analysis and that a multidimensional analysis was required. An early work involving low temperatures and two-dimensional CFD simulations of the fuel tanks did not use real jet fuel properties [5,6]. A mixture of glycerin and water was used to represent jet fuel. Although the viscosity of the mixture was varied to

Received 24 February 2006; revision received 12 January 2007; accepted for publication 24 January 2007.

*Graduate Student, Department of Mechanical and Aerospace Engineering, 300 College Park.

†Professor, Department of Mechanical and Aerospace Engineering and Group Leader, Modeling and Simulation, University of Dayton Research Institute, 300 College Park; jamie.ervin@notes.udayton.edu. Associate Fellow AIAA.

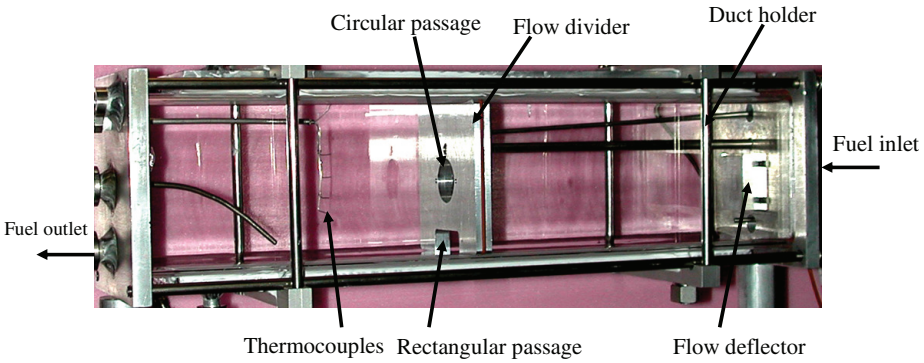

Fig. 1 Image of the quartz duct.

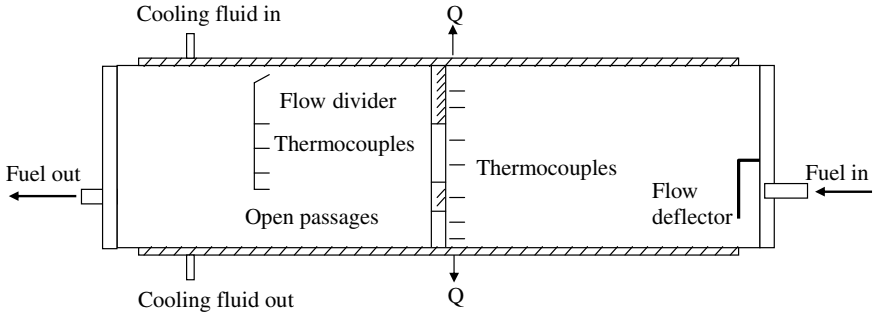

Fig. 2 Schematic of the quartz duct.

characterize the effect of freezing, the use of glycerin and water to represent jet fuel is likely not appropriate. Moreover, actual phase change itself was not simulated.

A recent study by one of the authors used two-dimensional CFD calculations to represent the actual solidification of fuel in an optical cell [3]. Real jet fuel properties were used, and the optical cell model involved a simple rectangular geometry. A momentum resistance source term was used to represent the flow resistance caused by crystal structures that were found to exist in liquid-solid regions. In addition, the flow was buoyancy driven due to temperature differences between the vertical cell walls. Although buoyancy-driven flow is dominant in some fuel tanks, forced flow is important in others. The fuel temperature and interaction between the solid particles and liquid are influenced by the flow rate. However, freezing behavior under forced flow has gone unstudied. Thus, it is important to numerically simulate the freezing of jet fuel under forced flow conditions. The enthalpy method has been used to simulate solidification in other work concerning simple mixtures in buoyancy-driven flow and is used in the present computations [7]. This method solves the energy equation that governs the heat transfer and phase change. It is also essential to study fuel solidification in a more intricate geometry because aircraft fuel tanks include internal structures (e.g., baffle plates, ribs, stringers) that may affect the overall heat transfer during the solidification process. An objective of the present work is to use a two-dimensional CFD model and temperature dependent fuel properties to simulate the solidification behavior of jet fuel in a forced flow.

In another previous work, the low-temperature behavior of jet fuels was studied in experiments where the fuel was chilled slowly for hours to maintain low temperatures within a fuel tank simulator [8,9]. The liquid fuel was discharged from the tank to determine the fraction of fuel holdup. (The mass of solidified and partially solidified fuel that cannot flow from the tank is referred to as the holdup.) However, CFD simulations concerning jet fuel solidification under forced flow conditions, which also have experimental validation, are not available. In addition, no published computational work has been found that incorporates jet fuel solidification in a geometry with one or more internal structures. This is due to the complexities of the low-temperature experiments and the involved multiphase transport. Therefore, in the present work, we have fabricated a quartz duct to study the effect of low temperatures on fuel flow, solidification, and holdup. The duct containing flowing fuel was subjected to temperatures below the freeze point[‡] of the jet fuel. The second objective of the present work is to use flow visualization and temperature measurements within the quartz duct to develop a better fundamental understanding of the freezing of jet fuel and to validate the numerical simulations.

II. Experimental

A. Flow Assembly

The accuracy of the computational results can be evaluated by comparing them with experimental measurements. Therefore, to validate the numerical simulations and to study the behavior of flowing jet fuel at low temperatures, a quartz duct (Figs. 1 and 2) was fabricated. The rectangular duct ($39.4 \times 8.9 \times 8.9$ cm) was fabricated from quartz because of its high optical quality and strength. Figure 1 shows an image of the duct that is separated into two compartments by a dividing plate similar to what might be encountered in some flow passages within a fuel tank. The dividing plate has two openings available for flow. One opening is circular (2.5 cm diameter) and located at the dividing plate center, whereas the other is rectangular (3.8×1.3 cm) at the plate bottom. The jet fuel flows into the duct through an inlet (1.3 cm diameter) located on one of the sidewalls. A deflector near the inlet redirects the inlet flow. In the absence of the deflector, much of the fuel entering through the inlet would essentially pass straightway through the circular opening on the dividing plate. It is presumed that this would result in inadequate mixing of the fuel. In addition, an outlet (1.3 cm diameter) is located at the opposite end of the chamber. Hollow aluminum plates are attached to both top and bottom surfaces. The plates are sealed on both the ends and allowed for threaded pipe fittings and mountings. By passing cooled methanol through these plates, the horizontal surfaces were cooled to the desired temperatures.

[‡]The freeze point (ASTM D2386) is actually a melting point and is determined by measurement of the temperature at which the last visible crystal melts upon heating of solidified fuel.

Table 1 Select low-temperature freezing experiments

Experiment no.	Fuel sample ID	Flow rate ml/ min	Chamber temperature, K	Chiller plates temperature, K
1	JP-8 (3804) JPTS (3775)	60	225	208
2	JP-8 (3804) JPTS (3775)	120	211	213

Table 2 Low-temperature jet fuel characteristics

Fuel	Freeze point, K	Pour point, K	Cloud point, K	ΔH, J/kg	f_s	ΔH_e, J/kg
JPTS (F3775)	218.7	210	214	4410	0.07	63,000
JP-8 (F3804)	224.9	215.2	221.2	4968	0.08	62,100
Jet A (F3219)	227.2	217.2	222.2	3487	0.06	58,117

Thermally conductive grease was applied to ensure good thermal contact between the quartz duct and plates.

The entire quartz duct was placed in an environmental chamber to simulate the low-temperature conditions existing in a high-altitude flight. A positive displacement pump forced fuel from an insulated reservoir (5 liter capacity) through the duct. A flow meter installed at the pump outlet monitored the fuel flow rate. The flow rates were selected to produce velocities similar to those found in aircraft fuel tanks of interest. A coil-type heat exchanger was used to cool the fuel before entering the duct. Fuel exited the duct through the outlet and passed through insulated tubing back to the reservoir. Two different neat jet fuel samples F3804 (JP-8) and F3775 (JPTS) were used in these experiments. Jet propellant-8 (JP-8) is widely used by the U.S. Air Force, and JPTS (jet propellant thermally stable) is a special purpose jet fuel and is known for high thermal stability and excellent low-temperature properties. Here, the alphanumeric designations (F3804 and F3775) refer to particular fuel samples used in the experiments and do not have any other meaning. The characteristics of these fuel samples are described in the subsequent sections.

Calibrated (type T) thermocouples were located inside the duct. Figure 2 shows a rake of seven thermocouples near the flow divider and another rake of five thermocouples near the center of the other compartment within the duct. Thus, temperature measurements on both sides of the flow divider were recorded. Thermocouples were installed in the fuel lines entering and exiting the duct, and the temperature of the methanol entering and leaving the chiller plates was also measured. The temperatures of the top and the bottom walls were recorded and later used as the boundary conditions for the CFD calculations. A pressure transducer measured the pressure drop between the inlet and outlet of the duct. All data was recorded using the data acquisition system (Personal DaqView PlusXL version 1.9) once every minute. Table 1 shows the select experiments that were performed and are discussed later in the results.

Lighting for the quartz duct consisted of an optical fiber panel that uniformly illuminated the cell. Polarizing filters on the front and back of the duct maximized the contrast between the solid and liquid fuel as cross polarization eliminated light transmittance through the liquid fuel. A high-resolution digital camera (Sony DKC-ST5, 4 megapixel) equipped with a zoom lens (Sony VCL1205B) was used to capture several images every 30 min. These images were used for area measurements of the frozen fuel for purposes of comparison with CFD calculations.

B. Low-Temperature Properties of Jet Fuels

To simulate jet fuel solidification, it is also important to study the effect of jet fuel properties and temperature on freezing. Although used for jet fuel specification, the fuel freeze-point temperature is not what dictates fuel flow to the boost pumps. Pumpability, or flowability, is limited by the fuel viscosity, which in turn, is related to the cloud-point and pour-point temperatures of the fuel. The cloud-point temperature (T_h) (ASTM D2500) is known as the temperature at which visible crystals first appear in a cooled fuel. The pour-point temperature (T_l) (ASTM D97) is defined as the lowest temperature at which the fuel still flows before entering a semirigid state. When the fuel reaches the pour-point temperature, it ceases to flow and is unavailable for use. The freeze-point, cloud-point, and the pour-point temperatures were measured using a Phase Technology Series 70V Petroleum Analyzer and are listed in Table 2. Although the crystallization dynamics of jet fuels is not well understood, it is known that the solidifying crystals essentially consist of larger normal alkanes. The crystallizing normal alkanes entrap other fuel species that remain in the liquid phase. The normal alkane distributions for two fuel samples, JPTS (F3775) and JP-8 (F3804), were measured by gas chromatography with mass spectroscopy (GC-MS) and are shown in Fig. 3 [10]. The individual normal alkane constituents in Fig. 3 add up to give the total normal alkane mass fraction of 0.274 for JPTS (F3775) and 0.238 for JP-8 (F3804).

CFD calculations involve the solution of governing equations that require low-temperature properties (density, viscosity, thermal conductivity, and specific heat) of jet fuels. Low-temperature properties of JP-8 (F3804) have been reported in our previous work and are used in the current simulations [3]. However, because the published properties of JPTS (F3775) are not available for temperatures below 233 K, measured values of specific heat and viscosity were obtained in the current work. In addition, temperature dependent values of density and thermal conductivity compiled by the Coordinating Research Council were used in all simulations [11]. Because the density and thermal conductivity vary linearly between 295 and 233 K, they were linearly extrapolated for temperatures below 233 K. During solidification, large normal alkanes increase in density by as much as 6% and because normal alkanes represent only a fraction of the total fuel mass, large variations in density are unexpected. Moreover, the extrapolated values of jet fuel thermal

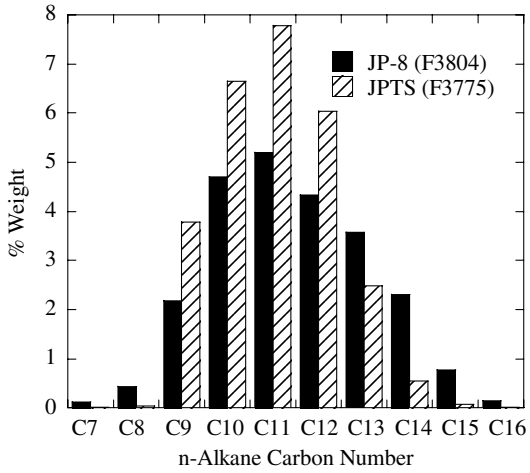

Fig. 3 Measured normal alkane distributions for JPTS (F3775) and JP-8 (F3804).

conductivity were compared with the thermal conductivities of individual normal alkane constituents. The extrapolated values of thermal conductivity agree well with the thermal conductivity of individual normal alkane constituents at their solidification temperatures [3]. Therefore, it is reasonable to accept the extrapolated values of thermal conductivity for temperatures below 233 K. The specific heat and viscosity were measured as a function of temperature and are described in the following paragraphs.

A differential scanning calorimeter (DSC) (TA Instruments, model 2920, cooling rate 1 K/ min) was used to determine the effective specific heat below 233 K for the fuel sample of JPTS (F3775). Figure 4a shows the measured specific heat for JPTS (F3775) for temperatures below 220 K. From Fig. 4a, it can be observed that the specific heat varies by less than 5% before solidification begins at $T_h = 214$ K. In contrast, it increases significantly after solidification is initiated. The specific heat is approximately 1700 J/kg · K at 214 K and increases to 5200 J/kg · K at 212 K due to continued cooling of the solidifying fuel. After the solidification is complete at 210 K (T_l), the specific heat is essentially constant again. Hence, it is reasonable to treat the specific heat as a constant (1700 J/kg · K) before the onset of freezing and as another constant (2750 J/kg · K) after the freezing is complete. Figure 4b shows the measured specific heat of JP-8 (F3804) for temperatures below 222 K [3]. The overall specific heat behavior of JP-8 is similar to that of JPTS, but the curve for JP-8 lies within a higher temperature range than that of JPTS.

Viscosity is one of the most important fuel properties to consider when studying the effect of low temperatures on fuel flow. Viscosity measurements of JPTS (F3775) were performed using a scanning

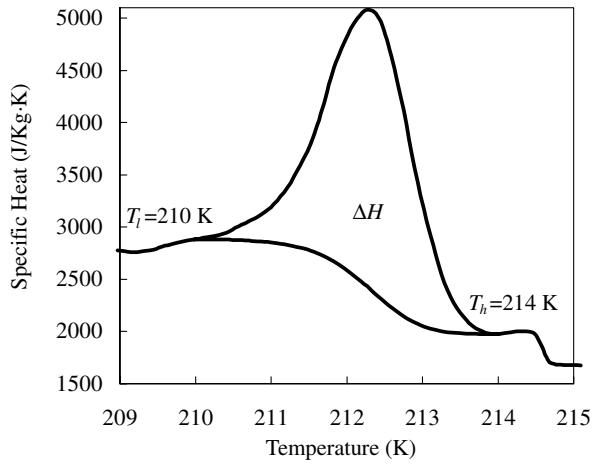

a)

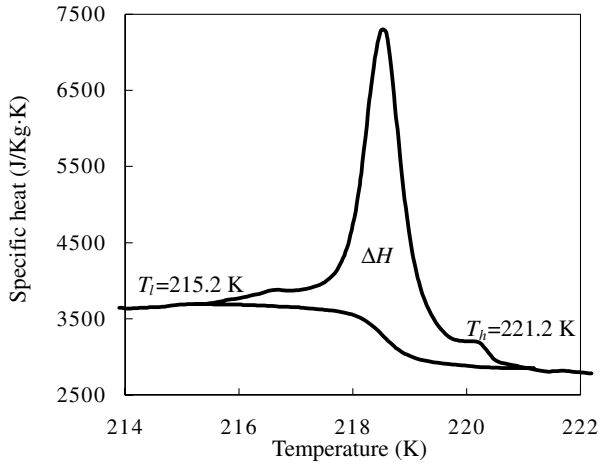

b)

Fig. 4 Measured specific heat for fuel samples a) F3775 (JPTS) and b) F3804 (JP-8).

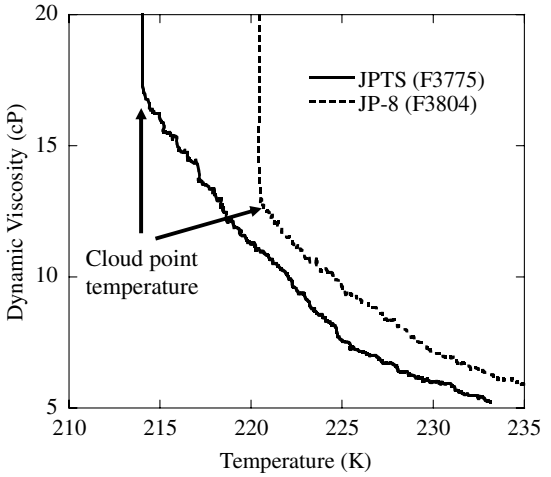

Fig. 5 Measured dynamic viscosity of JPTS (F3775) and JP-8 (F3804).

Brookfield Viscometer (Tannas, Plus Two). This technique offers the advantage of being able to measure dynamic viscosity as a function of temperature. As the fuel sample (30 ml) is cooled from 233 to 213 K at 5 K/h, the viscosity is measured continuously by the increasing torque generated by a spindle rotating in the fluid at constant speed (12 rpm). Figure 5 shows the measured dynamic viscosity of JPTS between 233 and 213 K, which is 3 K above $T_l = 210$ K of F3775. For temperatures between 213 and 210 K, the viscosity values were extrapolated for simplicity. Similarly, for JP-8, the viscosity measurements are shown for temperatures in the range between 233 and 220 K, which is approximately 5 K above the $T_l = 215.2$ K of F3804 [3]. Figure 5 shows that both fuels display a gradual increase in viscosity with decreasing temperatures. As the fuels approach their cloud-point temperatures (T_h), the viscosity increases rapidly. This sudden increase in viscosity is due to the onset of crystal formation at the cloud-point temperature [10]. The rise in viscosity also agrees with the rapid increase in specific heat at the cloud-point temperature and that the jet fuels solidify over a narrow temperature range. The viscosity measurements were calibrated with measurements obtained at −40°C using a glass capillary viscometer (ASTM D445) [12].

III. Simulation Methodology

Here, we use the enthalpy method to simulate solidification which follows the work of Voller and Prakash, and is outlined below [7]. With the enthalpy method, the solid-liquid mixture is characterized by the solid mass fraction f_s. The enthalpy within the solid-liquid region H is expressed as

$$H = h + \Delta H \tag{1}$$

where h is the sensible heat and

$$h - h_0 = \int_{T_0}^{T} C_p \, \mathrm{d}T$$

Here, C_p is the specific heat and h_0 is a reference enthalpy. In Eq. (1), ΔH is the heat of fusion and is written as a function of temperature

$$\Delta H = f(T) = \begin{cases} L & T > T_h \\ L(1 - f_s) & T_h \geq T \geq T_l \\ 0 & T < T_l \end{cases} \tag{2}$$

where T_h is the temperature at which the solid formation begins, T_l is the temperature at which freezing is complete, and L is the heat of fusion in the solid-liquid coexistence region.

The entire domain is treated as a porous medium, where the porosity λ has the following values

$$\lambda = (1 - f_s) = \begin{cases} 0 & \text{solid} \\ 0 < \lambda < 1 & \text{solid \& liquid} \\ 1 & \text{liquid} \end{cases} \quad (3)$$

The governing equations are written in terms of the superficial velocity (i.e., the ensemble-average velocity) defined as

$$\boldsymbol{u} = \lambda \boldsymbol{u}_f \quad (4)$$

where $\boldsymbol{u}_f$ is the actual fluid velocity vector.

In the solid-liquid coexistence region, solidifying structures form that may resist fuel flow. The flow in the solid-liquid region is represented by the D'Arcy relation [13]:

$$\boldsymbol{u} = -(K/\mu)\nabla P \quad (5)$$

In Eq. (5), K is the permeability that characterizes the ease with which a fluid flows under a pressure gradient through a porous material. K is determined by pore geometry and has a statistical distribution of sizes. Many empirical and semi-empirical representations for K exist, and the Kozeny relation [14] is often used

$$K = C_0 \lambda^3 / \Sigma^2 \quad (6)$$

where C_0 is a dimensionless constant that depends on the pore geometry and Σ is the interstitial surface area of the pores per unit volume of porous material. It is impractical to measure λ and Σ, and a simpler expression can be written as [7]:

$$K = \lambda^3 / C(1 - \lambda)^2 \quad (7)$$

where C is a constant and includes the effects of Σ, pore shape, size, and orientation. During the phase-change process, the value of C is assumed to depend on the morphology of the porous media and is referred to as the morphology constant. Equation (7) can be combined with Eq. (5) to give the superficial velocity in the solid-liquid phase region (For simplicity, here, the product $C\mu$ will be written as C^* using appropriate units) [7]:

$$\boldsymbol{u} = -\lambda^3 \nabla P / [C^*(1 - \lambda)^2] \quad (8)$$

Equation (8) shows that for the liquid phase, as the porosity λ approaches unity, pressure losses due to flow through the porous medium decrease to zero. Similarly, for the solid region, as the porosity approaches zero, the velocity decreases to zero. Moreover, as C^* is increased for a fixed μ, λ, and ∇P, Eq. (8) shows that the velocity decreases or the flow resistance increases. Thus for jet fuel, crystallization behaviors that inhibit flow would tend to have larger values of C^*.

Figure 4 shows that T_h and T_l are the measured cloud- and pour-point temperatures, respectively. The prediction of the solidified fuel mass which is unavailable for use is important, and by the definition of the pour point, the fuel does not flow at T_l. Hence, f_l between T_h and T_l can be estimated as

$$f_l = (T - T_l)/(T_h - T_l) \quad (9)$$

Therefore, f_l is one (all liquid) at temperatures above T_h, and, zero (all solid) at temperatures below T_l.

As normal alkanes precipitate from the solution, f_s increases while f_l, K, and λ decrease. Because it is difficult to measure λ within freezing jet fuel, λ has been assumed to be proportional to f_l, which is a function of temperature. The cloud-point and pour-point temperatures can be accurately measured as described earlier and hence, f_l can replace λ in Eq. (7) [3]. For convenience, f_l is normalized to vary between zero and one. Because there is large uncertainty in C of Eq. (10), it is acceptable to use the normalized value of f_l.

$$K = f_l^3 / [C(1 - f_l)^2] \quad (10)$$

The fuel enthalpy can be calculated by integrating the specific heat with respect to temperature. Thus, for the jet fuel sample JPTS (F3775), the confined area between T_h (214 K) and T_l (210 K) in Fig. 4a is an integrated value and represents the heat of fusion ΔH of precipitating normal alkanes. For the present JPTS sample, the measured heat of fusion ΔH is 4410 J/kg (enclosed area, Fig. 4a). Analytical phase-separation techniques [15] have shown that approximately 7% (mass) of the JPTS (F3775) sample actually solidifies at 210 K (T_l). Thus, for the JPTS (F3775) fuel sample, the maximum value of the solid fraction f_s is 0.07, which is approximately one-fourth of the total normal alkane distribution (0.274). The solid fraction of 0.07 corresponds to a minimum liquid fraction of 0.93. The measured heat of fusion is divided by f_s to calculate an effective heat of fusion ΔH_e.

$$\Delta H_e = \Delta H / f_s \quad (11)$$

Hence, $\Delta H_e = 63000$ J/kg. Similar DSC and gas chromatography-mass spectrometer (GC-MS) measurements of JP-8 (F3804) and Jet A (F3219) are listed in Table 2 [3]. It is observed that the specific heat behavior during phase change varies by $\pm 5\%$ among the fuel samples.

IV. Numerical Modeling

This section describes the numerical techniques used in all the simulations. A commercially available CFD code, CFD-ACE (ESI Group) was used to simulate the laminar, time-varying flow and heat transfer. In our previous work, the code was modified to treat solidification [3]. The unsteady Navier–Stokes and energy (enthalpy) equations were solved by a finite volume method. The temporal differencing was represented by a second order Crank–Nicolson scheme, and an upwind spatial differencing scheme was used [16]. A source-term based, fixed grid enthalpy method is used to implement the calculations [3,7].

A two-dimensional unstructured grid (Fig. 6) was employed for transient solution of the flow and heat transfer in the quartz duct. The boundary conditions for temperature come from a spatial average of the thermocouples located at discrete locations. These spatial averages are represented as functions of time and are used as transient temperature boundary conditions for the horizontal walls, whereas the vertical walls are assumed to be insulated. The initial measured fuel temperature is uniform. Figure 7 shows the temperature profile of the horizontal walls employed in the simulations of fuel cooling. The temperature profiles of the horizontal walls are different for both the jet fuel samples of JP-8 and JPTS due to differences in the temperature ranges of solidification for these fuel samples. The top

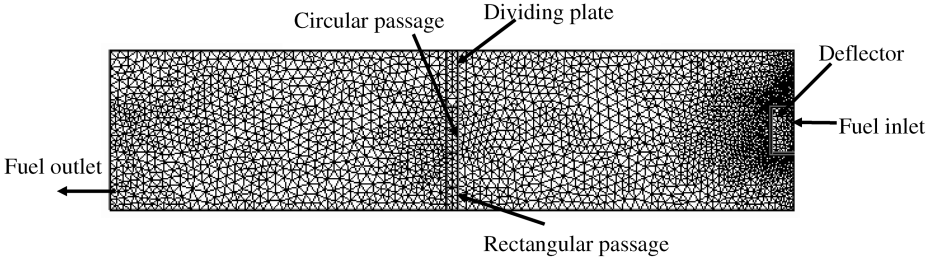

Fig. 6 Two-dimensional unstructured grid.

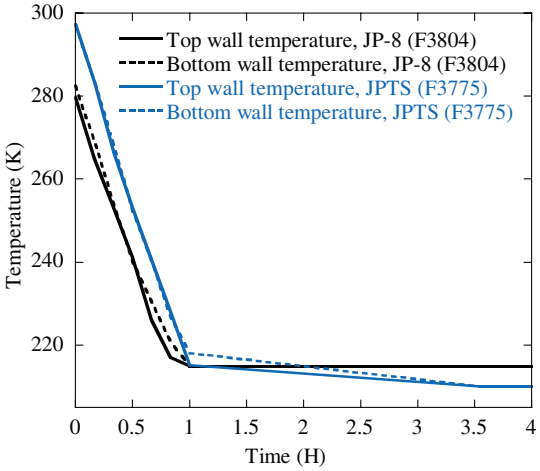

Fig. 7 Temperature schedule for the cooled horizontal walls used for freezing simulations.

and bottom walls decrease uniformly in time from 281 to 215 K for JP-8 (F3804) and from 297 to 210 K for JPTS (F3775) after 3 h.

As described earlier, temperature-dependent properties of JP-8 (F3804) and JPTS F3775) are used in the simulations as these fuels were used in the experiments. The internal structures of the duct are made of aluminum, and the properties of aluminum do not significantly change between the temperatures of interest here. Thus, constant properties of aluminum were used in all the simulations.

When the global error residuals were reduced below four orders of magnitude from their maximum values, the solution was considered to be converged. Table 3 describes the grid refinement study conducted to ensure the grid independence of the solution. The table shows temperatures and liquid fraction at three different locations in the duct after the fuel was cooled for 1.5 h. Results from a grid with 6932 cells were found to be grid independent and are described in this work. Further grid refinement resulted in negligible changes in the solutions.

V. Results and Discussions

Here, the computational and experimental results of jet fuel freezing in the quartz duct are reported. The effect of the morphology constant is studied and an optimum value of C^* is determined by numerical calculations. The simulations are validated with the help of temperatures and images recorded during the experiments. The images show the solidified area and the resulting crystal structures of jet fuels at different times. The effect of the freezing temperature and the influence of forced flow on phase change are described.

A. Experimental Validation and the Effect of C^* on Freezing

It was explained in earlier sections that flow resistance and the crystallization behavior of jet fuel are characterized in the current model by the value of C^*. Equation (8) elucidates the significance of C^* and that larger values of C^* reduce the liquid fuel flow through the two-phase region. Because C^* for the freezing of jet fuels cannot be directly measured, it is obtained by adjustment until agreement between the measured and calculated area of the solidified fuel is observed. The calculations were performed for three different values of C^*, which varied by several orders of magnitude.

Figures 8a–8c compare the effects of three different values of C^* (1, 1×10^5, and 1×10^{10} kg/m$^3 \cdot$ s, respectively) on the calculated solidified fuel area and the velocity profile. These figures show contour plots of the normalized liquid fraction and velocity vectors for JP-8 (F3804) in the glass duct after 2 h of cooling. The figures show that as the horizontal walls are cooled, a thick layer of solidified fuel develops at the top and bottom surfaces. (The size of a velocity vector is proportional to its magnitude, which varies over the range of 0–0.12 cm/s.) A black contour line in Figs. 8a–8c distinguishes the liquid from the solidified fuel. The contour line represents the liquid fraction $f_l = 0.93$ occurring at an average temperature of 220.8 K which is 0.4 K below the cloud-point temperature of F3804 (221.2 K). Considering a difference of 0.4 K (an error of 0.18%) negligible, it can be said that the contour line represents the cloud-point temperature. As stated earlier, the cloud-point temperature is the temperature at which solidified fuel is visible in the liquid fuel. Hence, the black contour line representing the cloud-point temperature demonstrates the capability of the model to calculate the correct profile of the solidifying structure.

Figure 8a represents a C^* value of 1 kg/m$^3 \cdot$ s and shows an uneven and abrupt solidified area. It also shows the maximum area occupied by frozen fuel, relative to Figs. 8b and 8c. The protruded area in Fig. 8a is caused by the flowing fuel in the liquid-solid region. It is evident that the velocity vectors in the region within the black contour line are larger in Fig. 8a. The protrusion decreases near the top and bottom walls when C^* is increased to 1×10^5 kg/m$^3 \cdot$ s (Fig. 8b). Also, smaller velocity vectors can be observed in Fig. 8b indicating less flow relative to Fig. 8a. This means that a lower value of C^* causes higher velocity in the liquid-solid region. A further increase in the value of C^* to 1×10^{10} kg/m$^3 \cdot$ s (Fig. 8c) shows that the solidified fuel area decreases, relative to Figs. 8a and 8b and the protrusion nearly vanishes. The area of solidified fuel confined within the black contour line in Fig. 8c is 12.9 cm^2, which is in agreement with the measured area (13.4 cm^2). (The uncertainty in the measured solidified area is ± 0.5 cm^2.) Thus, the calculated area represented by Fig. 8c best approximates the visualization image (Fig. 8d). Further increases in C^* did not yield improved predictions. Our previous study with buoyancy-driven flow also established the value of C^* as 1×10^{10} kg/m$^3 \cdot$ s for the JP-8 fuel sample [3].

Similar calculations were performed for the JPTS (F3775) fuel and comparisons were made with the visual images. C^* was varied from 1×10^5 to 1×10^{12} kg/m$^3 \cdot$ s to find an optimal value. As observed with the JP-8 fuel sample, calculations with a C^* value of 1×10^{10} kg/m$^3 \cdot$ s showed the greatest similarity with the images. Figures 9a and 9b show the solidified fuel area in the duct by means of an image and a simulation, respectively. Figure 9b shows the contour plot of JPTS (F3775) for a C^* value of 1×10^{10} kg/m$^3 \cdot$ s which gives a calculated solidified fuel area of 15.4 cm^2 and is in agreement with the measured area of 14.9 cm^2 (± 0.5 cm^2) of Fig. 9a. Both the figures show that the solidified fuel accumulates near the top and bottom surfaces. The mass of solidified fuel increases in time due to the low temperatures of the horizontal walls.

Because a C^* value of 1×10^{10} kg/m$^3 \cdot$ s gives the best agreement between the simulations and measurements, therefore, for all the other simulations in this paper, a value of $C^* = 1 \times 10^{10}$ kg/m$^3 \cdot$ s is used for both F3804 and F3775 fuel samples. As described earlier, the effective heat of fusion ΔH_e value is used to predict the solidification behavior. Because the effective heat of fusion is nearly

Table 3 Grid refinement study for the freezing model

Number of cells	Temperature, K (center)	% change	Temperature, K ($x = 28$ cm, $y = 1.5$ cm)	% change	Temperature, K ($x = 10$ cm, $y = 7.5$ cm)	% change	Normalized liquid fraction	% change
2679	224.7	——	221.8	——	224.3	——	0.9374	——
4786	224.8	0.05	222.1	0.14	224.5	0.09	0.9237	1.46
6932	224.9	0.05	222.3	0.09	224.6	0.05	0.9207	0.33
10,369	224.9	0	222.3	0	224.7	0.05	0.9196	0.12

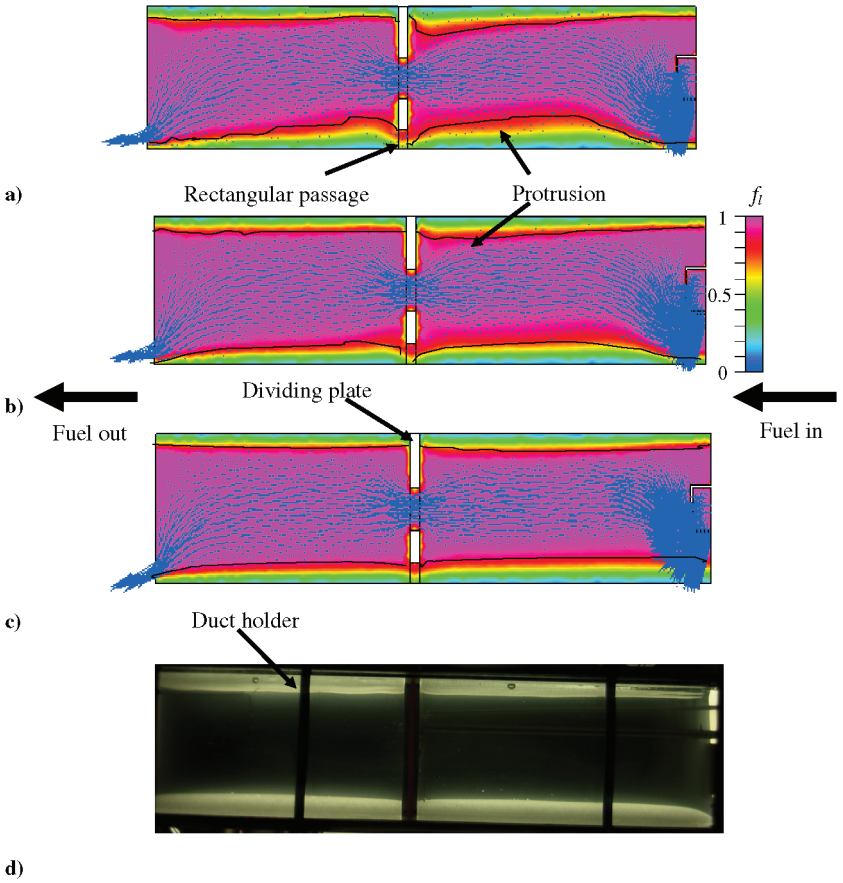

Fig. 8 Predicted liquid fraction and velocity vectors in the quartz duct after 2 h of cooling for JP-8 (F3804) at a flow rate of 60 ml/ min with $C^* =$ a) 1, b) 1×10^5, c) 1×10^{10} kg/m$^3 \cdot$ s, and d) visualization image.

the same for both the fuel samples, the same value of C^* provides convincingly similar results. The focus of this paper is on the use of JP-8 and JPTS. A few experiments and simulations were performed using a Jet A sample (Table 2). Low-temperature optical microscope images of crystals formed from the JP-8 and Jet A fuel samples were indistinguishable. In addition, the C^* value for the JP-8 and JPTS fuel samples was found to be the same as that of the Jet A sample.

However, detailed crystal structures of JP-8 and JPTS are also studied here and are found to be significantly different. The solidification of jet fuels involves complex molecular phenomena. The dynamic freezing process of jet fuel can be affected by several factors like crystal shape and size. Separate experiments were performed to study the crystal growth of JPTS (F3775) (Fig. 10a) and JP-8 (F3804) (Fig. 10b) fuels under forced flow conditions. For this study, the fuel flow rate was 120 ml/ min. These images represent the crystal structures that have grown from the bottom surface and extend into the bulk liquid fuel. Figure 10a (JPTS) shows long needlelike crystals that are closely grouped, whereas Fig. 10b (JP-8) shows solidified crystals in the form of fine plates that appear like a clustered arrangement. At later times, with a further decrease in temperature, jet fuel crystals grow and accumulate to further grow into the bulk. Because solidified jet fuel primarily consists of normal alkanes, the difference between the two crystal structures is believed to be due to differences in the normal alkane distribution (Fig. 3). The JPTS sample consists of 27.4% normal alkanes mostly ranging from C_9 to C_{14} and centered around C_{11}. In contrast, JP-8 fuel sample consists of 23.8% normal alkanes and has a wider distribution that ranges mostly from C_8 to C_{15}.

Although both JP-8 and JPTS fuel samples vary in their crystal microstructures, they require the same value of C^*. This indicates that the governing equations used for simulations here have certain

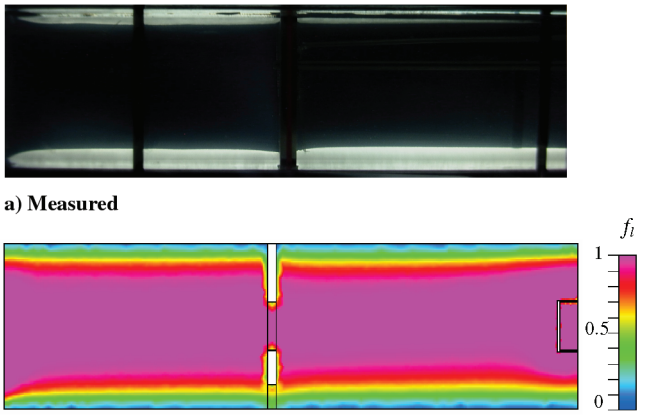

Fig. 9 Solidified fuel area in the quartz duct after 2 h of cooling for JPTS (F3775) at a flow rate of 60 ml/ min with $C^* = 1 \times 10^{10}$ kg/m$^3 \cdot$ s.

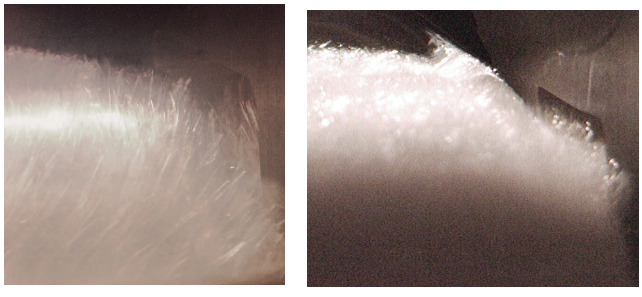

Fig. 10 Crystal structures of fuel samples of a) F3775 (JPTS) and b) F3804 (JP-8).

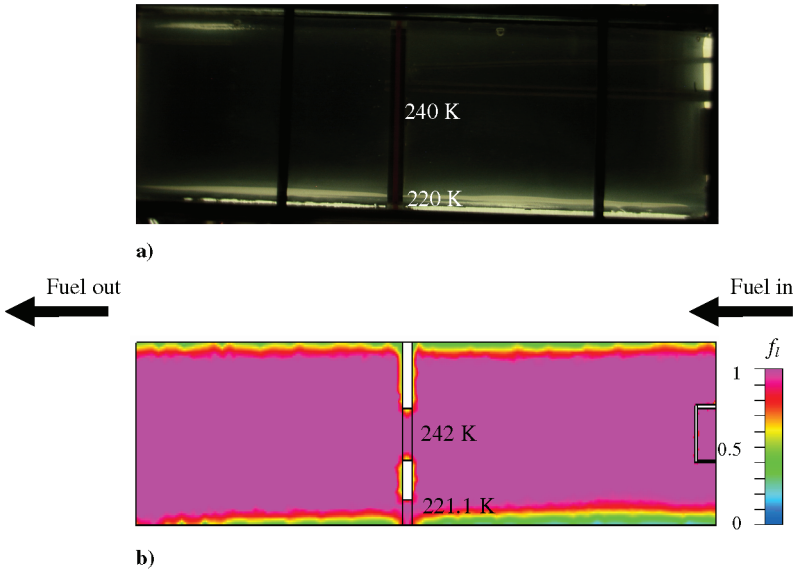

Fig. 11 Images of JP-8 (F3804) showing a) measured and b) calculated liquid fraction after 1 h of cooling and a flow rate of 60 ml/ min.

limitations and that includes their inability to capture small-scale details of the crystal microstructure. Nevertheless, this limitation is not fatal here, as the focus is on simulating the two-phase coexistence region and calculating the total solid fraction (holdup) and overall freezing behavior under forced flow conditions.

The region occupied by solid-liquid fuel matrix grows in time as the temperature decreases. Therefore, it is important to predict the increase in solidification with time and validate the solidified fuel area with measurements. Figure 11 provides further validation of the simulations by comparing them with the measured solidified fuel area using a C^* value of 1×10^{10} kg/m$^3 \cdot$ s. Figures 11a and 11b show images from the experiments and a calculated contour plot of liquid fraction, respectively. Both figures show the solidified area of JP-8 (F3804) after 1 h of cooling for an inlet fuel flow rate of 60 ml/ min. Figure 11 also shows the predicted and measured temperatures at two different locations. The temperature at a location near the center of the duct is 240 K, which is expectedly higher than the temperature near the bottom surface (220 K). These figures show good agreement between the measured and predicted temperatures (within 2 K). (The uncertainty in the measured temperature is ± 1 K.) As the cooling proceeds, the amount of frozen fuel trapped in the duct increases. Because colder fuel is more dense and tends to reach the bottom surface, the upper surface experiences the flow of relatively warmer fuel. The warm fuel near the upper surface reduces the growth rate of solidified fuel on the top surface. The relatively low temperatures of the horizontal surfaces results in the conduction of heat to the dividing plate. Therefore, for a location near the dividing plate, the temperature is lower due to increased heat transfer caused by the dividing plate. Because of the lower temperatures there, solidified fuel accumulates around the dividing plate.

To further validate the simulated temperatures and to study the thermal profile of the cooling fuel within the duct, the simulations are compared with the measurements. Figures 12a and 12b compare calculated and measured temperatures for the two fuels, JP-8 (F3804) and JPTS (F3775), respectively, using a C^* value of 1×10^{10} kg/m$^3 \cdot$ s. These plots show how the temperature varies with time at two different thermocouple locations. It can be observed that the calculations are in relatively close agreement with the measurements (within 3 K). Similar agreement was observed at other thermocouple locations in the duct. Calculated contour plots can be useful in representing a complete thermal profile in the duct at any specific time. Figures 13a and 13b show the calculated temperature contours and velocity vectors inside the glass duct after 10 min and 2 h of cooling, respectively. Both figures show relatively large velocity vectors at the inlet due to the expansion of the flow area after the inlet. Because Fig. 13a represents an earlier time, fuel temperature is relatively higher and there is no frozen fuel

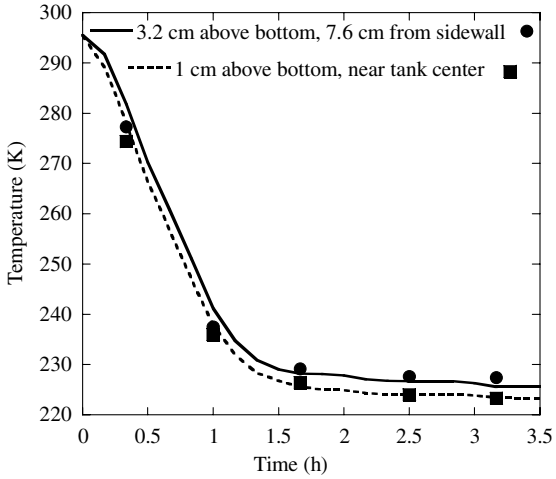

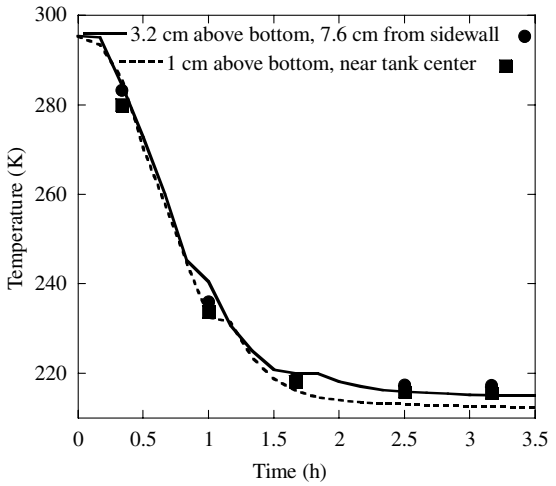

Fig. 12 Measured and simulated temperatures for the fuel samples of a) JP-8 (F3804) and b) JPTS (F3775) at two different thermocouple locations. The symbols represent measured temperatures.

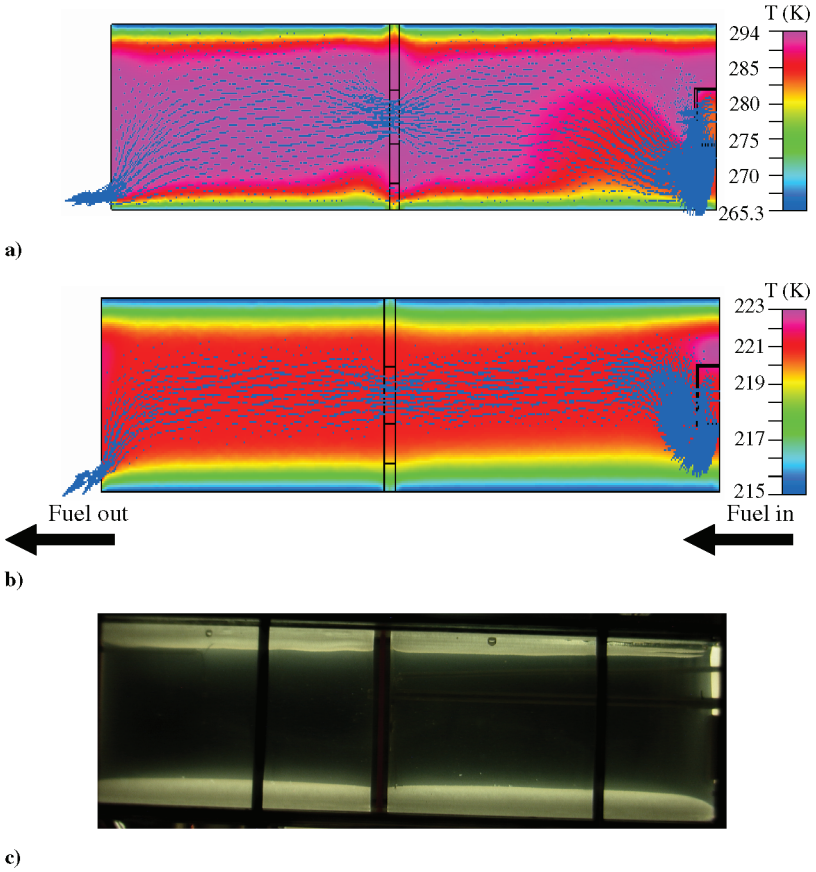

Fig. 13 Temperature contours and velocity vectors for JP-8 (F3804) in the quartz duct after a) 10 min and b) 2 h of cooling, and c) image of frozen fuel after 2 h and a flow rate of 60 ml/ min.

accumulated in the duct. Because of the absence of frozen fuel, the flow is unobstructed and the velocity vectors are larger and can be observed near the top and bottom surfaces of the duct. Figure 13b represents the temperature profile in the duct at a later time, and hence, the temperature of the fuel decreases (below the freeze point). Therefore, solidified fuel accumulates near the horizontal walls and the velocity vectors are not observed near the horizontal surfaces. As a result, the rectangular opening located at the bottom of the dividing plate is obstructed by the solidified fuel and restricts the flow through it. Hence, the fuel flows toward the outlet through the center opening only. Therefore, in the fuel tank design, an opening near the bottom should be made large enough to allow the fuel to flow through it. Because of limited flow passage, the velocity through the duct accelerates and increases by as much as a factor of four.

B. Effect of Fuel Flow Rate on Freezing

To study the effect of fuel flow rate on temperature and solidification profiles inside the duct, simulations were performed in which the inlet flow rate was varied. Four different fuel inlet velocities (0.80, 0.30, 0.15, and 0.08 cm/s) were selected for their influence on fuel solidification. Here, the results with the fuel inlet velocity of 0.80 and 0.08 cm/s are shown in Figs. 14 and 15. The wall temperatures followed the schedule of Fig. 7.

Figure 14 shows the calculated contour plots representing the liquid fraction of the jet fuel (F3775) in the duct after 2 h of cooling. Figure 14a shows that when the inlet velocity is 0.08 cm/s, the calculated fraction of solidified fuel in the duct is 0.0763. It is observed that the fraction of solidified fuel increased to 0.0896, 0.1054, and 0.130 when the fuel velocity is decreased to 0.30, 0.15, and 0.08 cm/s, respectively. Thus, when the fuel inlet velocity is relatively higher, the total solid fraction in the duct is lower. This result is expected because when the fuel velocity is lower, the fuel remains in the duct for a comparatively longer period and, consequently, is subjected to lower temperatures for a longer residence time. Because higher fuel velocities show a decrease in the accumulation of the solidified fuel, it is beneficial to have higher fuel velocities in the fuel tanks. Figure 14a shows that higher velocities result in a more disordered and jagged layer of the solidified fuel along the horizontal surfaces. Also, due to higher inlet velocity, the bottom surface immediately below the deflector does not show any accumulation of the frozen fuel. Moreover, the rectangular opening at the bottom remains unblocked and high flow rate creates an uneven solidified fuel layer near the bottom surface. Therefore, the overall area of solidified fuel near the bottom surface is less than that at the top surface. In contrast, with decreased fuel velocity (0.08 cm/s), the solidified fuel area near bottom surface becomes smoother (Fig. 14b). Also, the rectangular opening near the bottom surface is nearly blocked due to accumulation of the solidified fuel.

Figures 15a and 15b show the temperature profiles in the duct when the fuel inlet velocities are 0.80 and 0.08 cm/s, respectively. It is observed that the overall fuel temperature inside the duct increases by approximately 3 K when the inlet velocity is 0.08 cm/s relative to when the inlet velocity is 0.80 cm/s. It can also be observed that the temperature profiles near the top and the bottom surfaces show similarity with the figures showing solidified fuel area (Fig. 14). Figure 15a shows that higher velocity causes more stratification of fuel in the duct, relative to that observed in Fig. 15b. Also, higher velocities do not allow cold fuel to settle at the bottom surface, resulting in more mixing and an uneven thermal profile near the bottom surface. In contrast to Fig. 15a, Fig. 15b shows a smoother or nearly flat temperature contour near the bottom surface, which is due to the lower fuel inlet velocity.

VI. Conclusions

In this work, the low-temperature behavior of jet fuels under forced flow conditions was studied using a quartz duct. Experiments and simulations were performed to explore the effect of different flow conditions on jet fuel freezing and the effect of solidification on

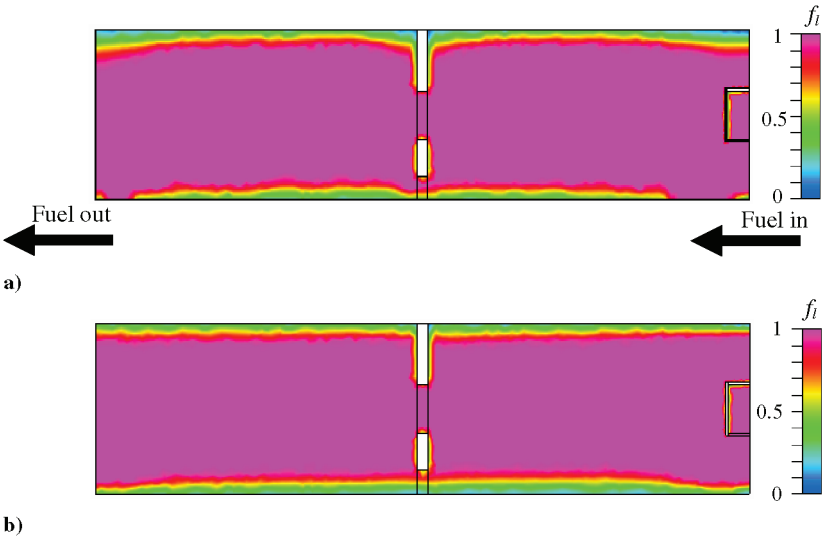

Fig. 14 Predicted liquid fraction of JPTS (F3775) in the duct after 2 h of cooling for an inlet velocity of a) 0.8 cm/s and b) 0.08 cm/s.

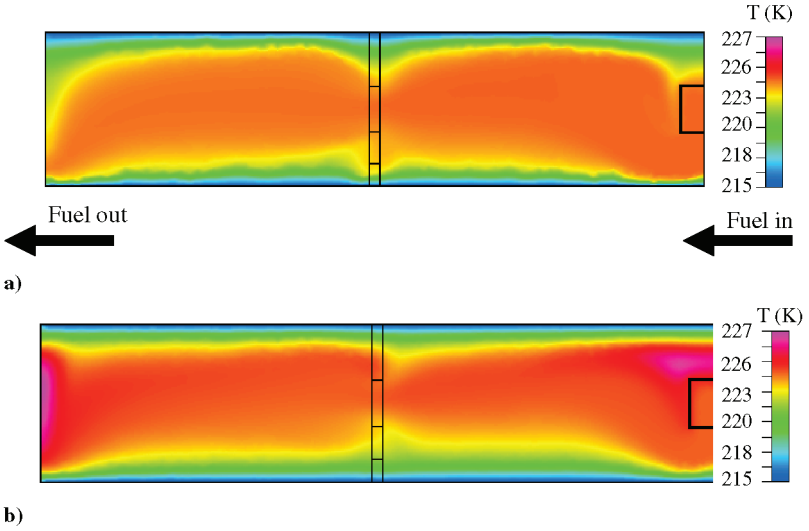

Fig. 15 Predicted temperature profile of JPTS (F3775) in the duct after 2 h of cooling for an inlet velocity of a) 0.8 cm/s and b) 0.08 cm/s.

fuel flow behavior. Two different jet fuel samples (JP-8 and JPTS) were used in the experiments and measured jet fuel properties were used in the simulations. The DSC and GC-MS measurements provided specific heat values and the enthalpy method was used to calculate the holdup due to freezing. The value of the morphology constant for both the fuel samples was obtained by adjustment until agreement between the measured and calculated area of the solidified fuel was observed.

The values of morphology constant for both fuel samples were found to be the same (1×10^{10} kg/m$^3 \cdot$ s). However, the observed crystal structures of JP-8 and JPTS were found to be very different. This means that the enthalpy method used here has certain limitations. The enthalpy method depends on the effective heat of fusion (ΔH_e), and because that value is nearly same for both the fuel samples, the calculations predicted the same value of C^*. Although this method can be successfully used to simulate the overall flow and heat transfer behavior in the solid-liquid region, the enthalpy method cannot predict the details of the crystal structure. This limitation cannot be considered fatal for this study because here the focus is on the overall flow, heat transfer, and freezing behavior of jet fuels.

Horizontal walls that were cooled down to the pour-point temperature of jet fuel showed significant accumulation of solidified fuel. Because of the increase in solidification at later times, the velocity vectors inside the duct showed that fuel ceased to flow through the rectangular opening at the bottom. Moreover, the dividing plate in the center of the duct acted as a thermal conductor and increased the holdup of the frozen fuel. Therefore, it is recommended to make larger passages near the bottom walls in the aircraft fuel tank and to optimize the design of fuel tanks such that they have minimum internal structures. Simulations of the effect of varying flow rates showed that lower flow rates resulted in more accumulation of solidified fuel inside the duct. Predicted temperatures and solidified area of fuel inside the duct were found to be reasonably similar to the measurements. Hence, it can be concluded that CFD can be an effective tool to simulate the flow and heat transfer of jet fuels at freezing temperatures under forced flow conditions.

Acknowledgments

This material is based on research sponsored by U.S. Air Force Research Laboratory under agreement number F33615-03-2-2347. The U.S. Government is authorized to reproduce and distribute reprints for Governmental purposes notwithstanding any copyright notation thereon. The views and conclusions contained herein are those of the authors and should not be interpreted as necessarily representing the official policies or endorsements, either expressed or implied, of the Air Force Research Laboratory or the U.S. Government.

References

[1] Coutinho, J. A. P., "Thermodynamic Model for Predicting Wax Formation in Jet and Diesel Fuels," *Energy and Fuels*, Vol. 14, No. 3, 2000, pp. 625–631.

[2] Beckermann, C., and Viskanta, R., "Mathematical Modeling of Transport Phenomena During Alloy Solidification," *Applied Mechanics Reviews*, Vol. 46, No. 1, 1993, pp. 1–27.

[3] Atkins, D. L., Ervin, J. S., and Saxena, A., "Computational Model of the Freezing of Jet Fuel," *Journal of Propulsion and Power*, Vol. 21, No. 2, 2005, pp. 356–367.

[4] McConnell, P. M., Desmarais, L. A., and Tolle, F. F., "Heat Transfer in Airplane Fuel Tanks at Low Temperatures," American Society of Mechanical Engineers Paper 83-HT-102, 1983.

[5] McConnell, P. M., Owens, S. F., and Kamin, R. A., "Prediction of Fuel Freezing in Airplane Fuel Tanks of Arbitrary Geometry: Part 1," *Aircraft Engineering*, Vol. 58, No. 9, 1986, pp. 20–23.

[6] McConnell, P. M., Owens, S. F., and Kamin, R. A., "Prediction of Fuel Freezing in Airplane Fuel Tanks of Arbitrary Geometry: Part 2," *Aircraft Engineering*, Vol. 58, No. 10, 1986, pp. 2–7.

[7] Voller, V. R., and Prakash, C., "Fixed Grid Numerical Modeling Methodology for Convection-Diffusion Mushy Region Phase-Change Problems," *International Journal of Heat and Mass Transfer*, Vol. 30, No. 8, 1987, pp. 1709–1719.

[8] Mehta, H. K., and Armstrong, R. S., "Detailed Studies of Aviation Fuel Flowability," Boeing Commercial Aircraft Co., NASA CR-174938, 1985.

[9] Stockemer, F. J., "Experimental Study of Low Temperature Behavior of Aviation Turbine Fuels in a Wing Tank Model," NASA CR-159615, 1979.

[10] Atkins, D. L., Ervin, J. S., and Shafer, L., "Experimental Studies of Jet Fuel Viscosity at Low Temperatures, Using a Rotational Viscometer and an Optical Cell," *Energy and Fuels*, Vol. 19, No. 5, 2005, pp. 1935–1947.

[11] "Handbook of Aviation Fuel Properties," Coordinating Research Council TR 530, Atlanta, GA, April 2004.

[12] Zabarnick, S., and Vangness, M., "Properties of Jet Fuels at Low Temperature and the Effect of Additives," *Preprint: American Chemical Society, Division of Petroleum Chemistry*, Vol. 47, No. 3, 2002, pp. 243–246.

[13] D' Arcy, H., Les Fontainer Publiques de la Ville de Dijon, Dalmont, Paris, 1856.

[14] Kozeny, J. S., "Ueber Kapillare Leitung des Wassers im Boden," Sitzungsberichte, Akademie der Wissenschaften Wien, Mathematisch-Naturwissenschaftliche, Vol. 136, Vienna, 1927, pp. 271–306.

[15] Moynihan, C. T., Mossadegh, R., and Bruce, A. J., "Determination of the Mass Fraction of Crystals in Partly Frozen Hydrocarbon Fuels," *Fuel*, Vol. 63, No. 3, 1984, pp. 378–384.

[16] "CFD-ACE (U) Users Manual," CFD Research Corp., Huntsville, AL, 2002.

L. Maurice
Associate Editor